Relative Contribution of Moisture Transport during TC-Active and TC-Inactive Periods to the Precipitation in Henan Province of North China: Mean State and an Extreme Event⬚

YANGRUIXUE CHEN,[a,b] BO LIU ,[b,c] YALI LUO,[d,e] CRISTIAN MARTINEZ-VILLALOBOS,[f,g] GUOYU REN,[c,h]
YONGJIE HUANG,[i] SIHAN ZHANG,[c] YONG SUN,[j] AND ZHONGSHI ZHANG[c]

[a] *Plateau Atmosphere and Environment Key Laboratory of Sichuan Province, School of Atmospheric Sciences, Chengdu University of Information Technology, Chengdu, China*
[b] *State Key Laboratory of Severe Weather, Chinese Academy of Meteorological Sciences, Beijing, China*
[c] *Department of Atmospheric Science/Centre for Severe Weather and Climate and Hydro-Geological Hazards, China University of Geosciences, Wuhan, China*
[d] *Collaborative Innovation Center on Forecast and Evaluation of Meteorological Disasters, NUIST, Nanjing, China*
[e] *Fujian Key Laboratory of Severe Weather, and Key Laboratory of Straits Severe Weather, China Meteorological Administration, Fuzhou, China*
[f] *Faculty of Engineering and Sciences, Universidad Adolfo Ibañez, Peñalolen, Santiago, Chile*
[g] *Data Observatory Foundation, Santiago, Chile*
[h] *Laboratory for Climate Studies, National Climate Center, China Meteorological Administration, Beijing, China*
[i] *Center for Analysis and Prediction of Storms, University of Oklahoma, Norman, Oklahoma*
[j] *State Key Laboratory of Tibetan Plateau Earth System, Resources and Environment, Institute of Tibetan Plateau Research, Chinese Academy of Sciences, Beijing, China*

(Manuscript received 2 August 2022, in final form 7 January 2023)

ABSTRACT: A Lagrangian model—the Hybrid Single-Particle Lagrangian Integrated Trajectory model (HYSPLIT)—is used to quantify changes in moisture sources and paths for precipitation over North China's Henan Province associated with tropical cyclone (TC) over the western North Pacific (WNP) during July–August of 1979–2021. During TC-active periods, an anomalous cyclone over the WNP enhances southeasterly and reduces southwesterly moisture transport to Henan. Accordingly, compared to TC-inactive periods, moisture contributions from the Pacific Ocean (PO), eastern China (EC), and the local area (Local) are significantly enhanced by 48.32% (16.73% versus 11.28%), 20.42% (9.44% versus 7.84%), and 2.89% (4.91% versus 4.77%), respectively, while moisture contributions from the Indian Ocean (IO), Southwestern China (SWC), Eurasia (EA), and the South China Sea (SCS) are significantly reduced by −31.90% (8.61% versus 12.64%), −16.27% (4.60% versus 5.50%), −8.81% (19.10% versus 20.95%), and −6.92% (12.18% versus 13.09%). Furthermore, the moisture transport for a catastrophic extreme rainfall event during 17–22 July ("21·7" event) influenced by Typhoon Infa is investigated. Compared to the mean state during TC-active periods, the moisture contribution from the PO was substantially increased by 126.32% (37.87% versus 16.73%), while that from IO significantly decreased by −98.26% (0.15% versus 8.61%) during the "21·7" event. Analyses with a bootstrap resampling method show that moisture contributions from the PO fall outside the $+6\sigma$ range, for both the TC-active and TC-inactive probability distributions. Thus, the "21·7" event is rare and extreme in terms of the moisture contribution from the PO, with the occurrence probability being less than 1 in 1 million times.

SIGNIFICANCE STATEMENT: Henan, one of the most populated provinces in China, experienced a catastrophic extreme precipitation event in July 2021 (the "21·7" event), coinciding with the activity of a tropical cyclone (TC) over the western North Pacific, which helps establish the moisture channel. Using a Lagrangian model, we provide a better understanding of how moisture transport changes associated with TC for the mean state of 1979–2021, and reveal how extreme is the moisture transport for the "21·7" event with the bootstrap technique. It is found that during active TC periods, the moisture contribution from the Pacific Ocean (the Indian Ocean) is significantly enhanced (reduced). For every 1 000 000 six-day events, less than one instance like the "21·7" event should be expected.

KEYWORDS: Lagrangian circulation/transport; Extreme events; Precipitation; Moisture/moisture budget

1. Introduction

During 17–22 July 2021, the Henan Province, located in North China (black quadrilateral area in Fig. 1a) experienced a catastrophic extreme rainfall event ("21·7" event, hereafter), with maximum daily rainfall reaching 624.1 mm at the Zhengzhou station (purple pentagram in Fig. 1b). Such rainfall amount accounted for 97.4% of the climatological annual precipitation of Zhengzhou, leading to over 300 deaths and more than $1.5 billion economic losses (https://en.wikipedia.org/wiki/2021_Henan_floods). The "21·7" event occurred during the rainy season of North China (RSNC), which is one of the three major monsoon rainy seasons in China (Ding and Chan 2005). Due to a usually weaker moisture transport along a longer transport channel, the total rainfall amount
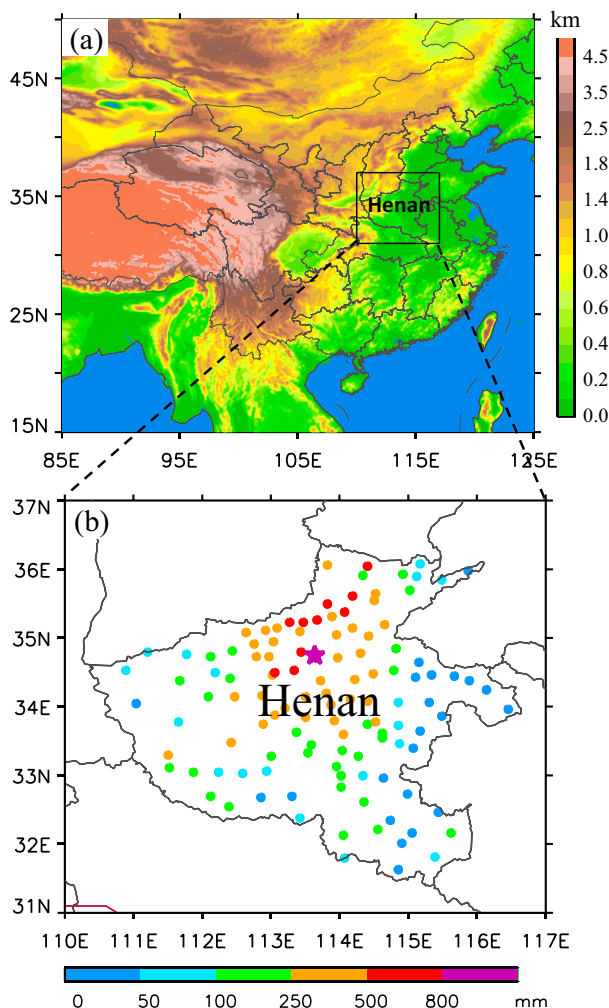
FIG. 1. (a) Topography (shaded) over east Eurasia and adjacent oceans, with Henan Province of China labeled. The gray curves indicate the province boundaries of China. (b) Distribution of the accumulated rainfall over Henan Province during the "21·7" event. The pentagram indicates the Zhengzhou station.

of the RSNC is relatively low, compared with the other two monsoon rainy seasons, i.e., the presummer rainy season over South China and the mei-yu season over central East China. However, rainfall events during the RSNC can also be featured with high intensity (Luo et al. 2016), occasionally causing disasters, e.g., the "7·21" (21 July 2012) Beijing extreme rainfall (Zhang et al. 2013), and both the "75·8" (5–7 August 1975; Ding 2015) and "21·7" extreme rainfall event over Henan Province (Luo et al. 2023; Yin et al. 2022). Coincidentally, the occurrences of such heavy rainfall events are often accompanied by the activity of tropical cyclones (TCs) over the western North Pacific (WNP) (Wen et al. 2015; Yang et al. 2017; Yin et al. 2022), which helps establish and strengthen the moisture channels for the precipitation processes during these events.

The influence of TCs on rainfalls has been extensively studied over many regions, e.g., North America (Prat and Nelson 2013, 2016), Middle America (Jiang and Zipser 2010; Franco-Díaz et al. 2019), Australia (Villarini and Denniston 2016), North Atlantic (Rodgers et al. 2001), and East Asia (Ren et al. 2006; Chang et al. 2013; Chen et al. 2017; Liu and Wang 2020). In addition to the production of extreme rainfall in a TC's circulation, TCs can also significantly influence distant rainfall by modulating the moisture channel and affecting circulation patterns (e.g., Schumacher et al. 2011; Yoshida and Itoh 2012; Bao et al. 2015; Wang et al. 2015; Deng et al. 2017; Arakane et al. 2019). In East Asia, TCs over the WNP can significantly influence the position and intensity of the western North Pacific subtropical high (WNPSH), which is closely related to the moisture transport over eastern China in the warm season (Ding and Chan 2005). The contribution of TCs to the regional water budget can be comparable with other contributors (Guo et al. 2017), such as the mean circulation of the East Asia summer monsoon. Significant differences in moisture budgets along the boundaries of the eastern China monsoon region have been found between TC days and non-TC days, i.e., days with and without the presence of TCs over WNP, respectively (Lin et al. 2017). About 80% of the water vapor transport are via the eastern boundary of the eastern China monsoon region during TC days, while for non-TC days most moisture inflows are via the southern boundary. The aforementioned studies suggest that TCs could have a substantial impact on the water cycle in East Asia. However, how moisture sources and paths for precipitation over North China, including Henan Province, would change associated with TC activities is not well understood.

To identify the quantitative moisture contribution of various factors or different moisture sources for the rainfall over a certain area, Lagrangian methods have recently been developed and successfully applied around the world (e.g., Gustafsson et al. 2010; Izquierdo et al. 2012; Salih et al. 2015; Huang and Cui 2015a,b; Sun and Wang 2014; Chen and Luo 2018; Nieto et al. 2019; Shi et al. 2020; S. Zhang et al. 2021). While air parcels of a target precipitation region cannot be traced back to the possible source regions in an Eulerian frame, the analysis based on a Lagrangian method can determine the trajectories of the air parcels and then estimate the moisture contribution of each source to the target area quantitatively. Despite this advantage, the use of Lagrangian methods to understand the TC influence on the moisture transport for rainfall over the Henan Province has received limited attention in the literature.

In this study, we aim to quantify the changes in large-scale circulation and, more importantly, the moisture paths and sources associated with TCs for precipitation in Henan during RSNC (July–August). To achieve this goal, we focus on a comparison between periods with and without TCs over the WNP, and adopt the Lagrangian methodology to better understand the moisture sources for both the mean state during 1979–2021 and the "21·7" event. The layout of this paper is as follows. Section 2 describes the data and methodology; section 3 illustrates the influence of TCs on the moisture paths and sources for Henan rainfall in the mean state. This is followed by a case study of the "21·7" event in section 4, with a discussion on how extreme the moisture transport was, compared to historical data; section 5 provides the concluding remarks.

2. Data and method

The TC best track data, covering the period of 1979–2021, are obtained from the Shanghai Typhoon Institute of China Meteorological Administration (https://tcdata.typhoon.org.cn/zjljsjj_zlhq.html). This dataset provides essential information on each TC over the WNP, including its name, position, center pressure, and maximum sustained winds at 6-h intervals. Following Zhong et al. (2019), only those TCs reaching tropical storm intensity (maximum sustained wind speed ≥ 17.2 m s^{-1}) were selected for this study. To investigate the influence of TC on circulation patterns and the associated moisture flux, we define a TC-active period when a TC is observed over the WNP (west of 150°E) and a TC-inactive period when no TCs over the WNP.

The Lagrangian model named the Hybrid Single-Particle Lagrangian Integrated Trajectory model (HYSPLIT) (Stein et al. 2015) (https://www.arl.noaa.gov/hysplit) is used to carry out the moisture backward tracking experiments. The latest reanalysis dataset of ECMWF—ERA5 (Hersbach et al. 2020)—was used to analyze the circulation and also as the input data for HYSPLIT. The variables are at 6-h intervals with a horizontal resolution of 0.25° and 37 vertical levels from 1000 to 1 hPa, including geopotential height, zonal and meridional winds, vertical pressure velocity, and specific humidity. Note that to minimize the influence of complex terrain over the regions moisture trajectories passing through, the ERA5 data with the highest horizontal resolution, i.e., 0.25°, are used.

The air parcels released over the target area, i.e., Henan Province, with 89 grids (Fig. S1 in the online supplemental material) at 5 vertical levels above ground (500, 1500, 3000, 5000, and 9000 m), which roughly correspond to 925, 850, 700, 500, and 300 hPa, are tracked backward every 6 h to obtain a good representation of the moisture pathways. Every trajectory calculation is run for 10 days, which is the approximate time that moisture remains in the atmosphere (Eagleson 1970). As a result, we identify 4 745 480 trajectories during July–August 1979–2021. Only effective trajectories with a decrease of specific humidity during the last 6 h before arriving at the target (the initial) grid are taken into consideration. In total, 1 892 837 effective trajectories are obtained, with 985 439 trajectories falling in TC-active periods and 907 398 trajectories in TC-inactive periods. We then calculate the trajectory frequency in a 1° × 1° grid box as the ratio of the number of effective trajectories passing through the grid cell to the total number of effective trajectories. As the trajectories might intersect the lowest level, i.e., the ground, of the input data, the trajectories would continue along the surface until they depart from the ground by a vertical motion or a terrain drop-down (Draxler and Hess 1998), and hence, the moisture transport in the abundant moisture regions of the lowest part of the troposphere is adequately considered.

Since an air parcel may experience multiple cycles of moisture gain and loss during its pathway from the source area to the target area, the source attribution method proposed by Sodemann et al. (2008) is used to calculate the moisture contribution of the relevant sources to the target area. This method was successfully used in several previous studies
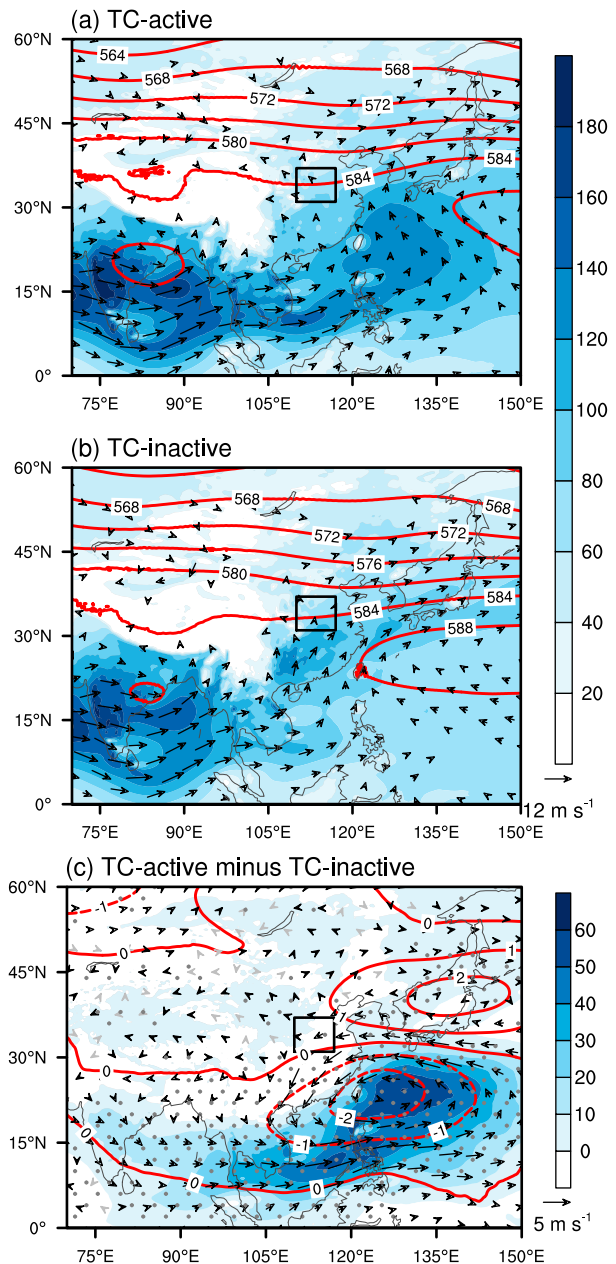

FIG. 2. Spatial distributions of mean geopotential height (contours; unit: dagpm) at 500 hPa, moisture flux (shading; unit: 10^{-3} m s^{-1} kg kg^{-1}), and horizontal wind fields (vectors; unit: m s^{-1}) at 850 hPa over East Asia during the (a) TC-active and (b) TC-inactive periods of 1979–2021, and (c) the associated difference between the TC-active and TC-inactive periods. Dotted regions in (c) present the 99% confidence level for geopotential height at 500 hPa and moisture flux at 850 hPa, and black vectors in (c) present the 99% confidence level for horizontal wind fields at 850 hPa based on Student's t test. The black solid rectangle indicates the location of Henan Province as presented in Fig. 1b.
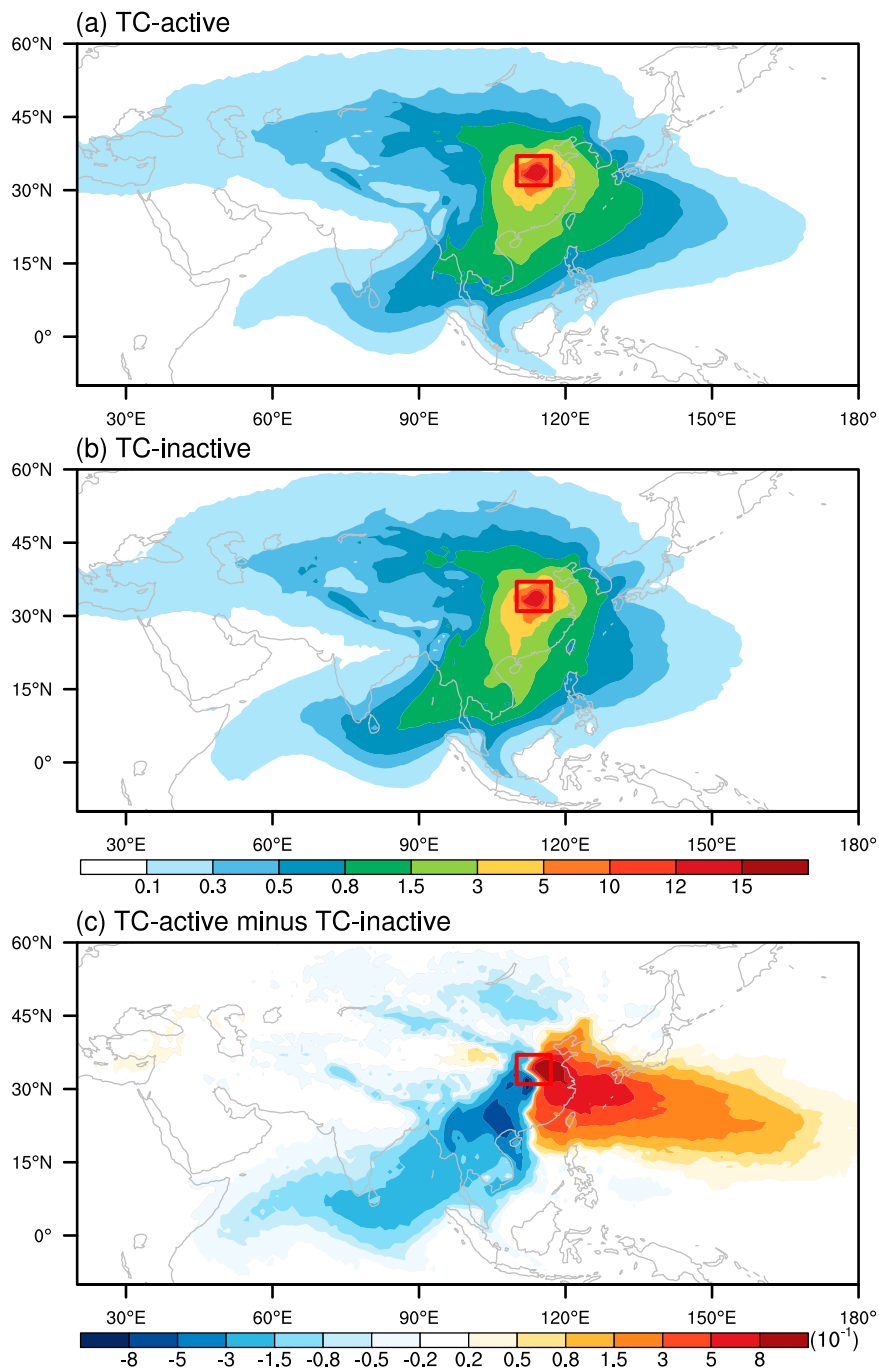
FIG. 3. Spatial distribution of the effective trajectory frequency (shading; unit: %) during the (a) TC-active periods and (b) TC-inactive periods of 1979–2021, and (c) the associated difference between the TC-active periods and TC-inactive periods of 1979–2021. The red rectangle indicates the target area presented in Fig. 1b.

(e.g., Sodemann and Stohl 2013; Martius et al. 2013; Huang and Cui 2015a,b; Chen and Luo 2018; S. Zhang et al. 2021). The details of this method are as follows.

As Stohl and James (2004, 2005) suggested, the moisture budget of an air parcel along the trajectory can be expressed as the balance between changes in moisture content $[m(\Delta q_a/\Delta t)]$

and "evaporation minus precipitation $(e_a - p_a)$," which can be written as follows:

$$e_a - p_a = m\frac{\Delta q_a}{\Delta t},\qquad(1)$$

$$\Delta q_t = q_t - q_{t-\Delta t},\qquad(2)$$

(a) TC-active

(b) TC-inactive

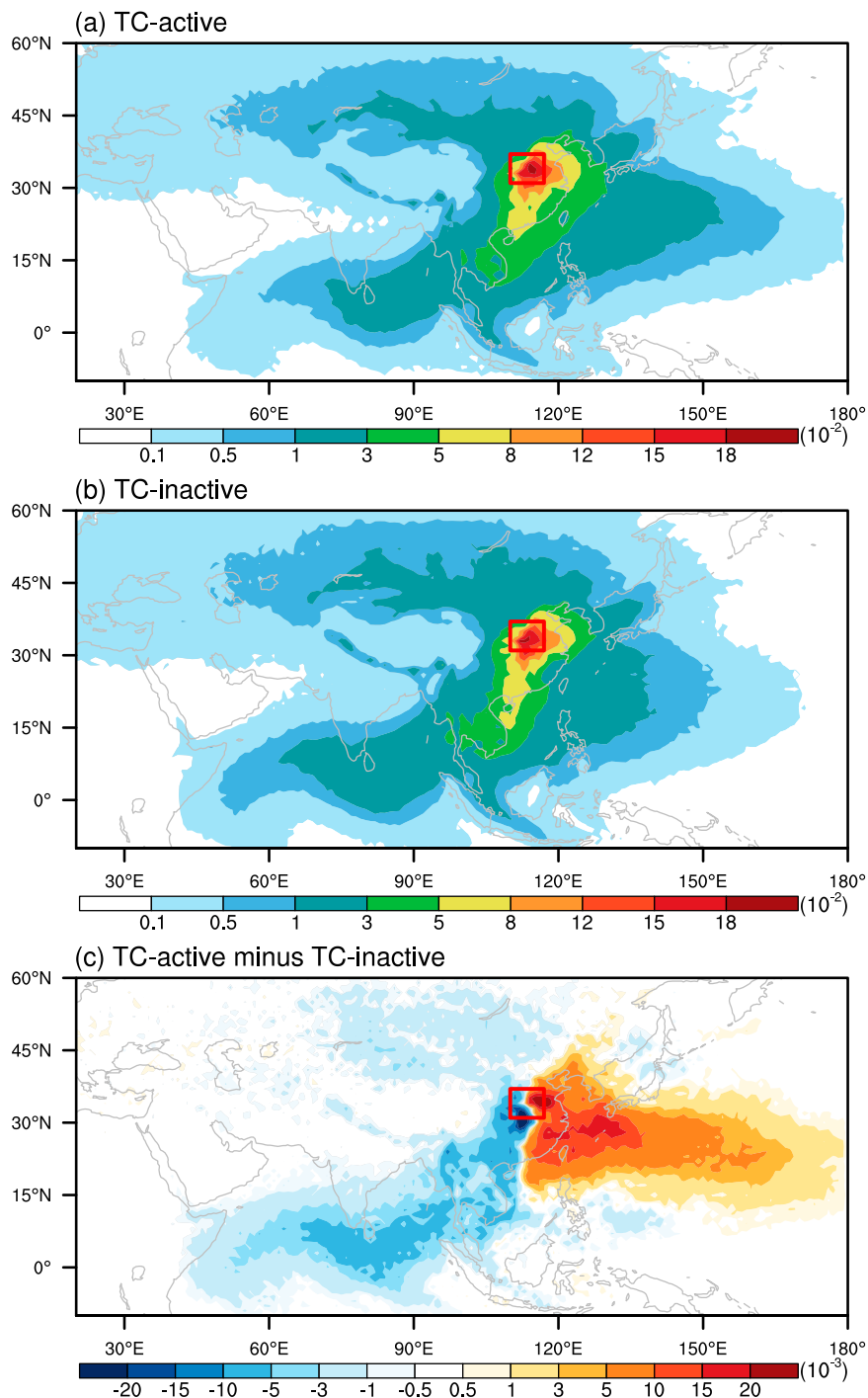

(c) TC-active minus TC-inactive

FIG. 4. The moisture contribution (shading; units: %) to precipitation over Henan Province during the (a) TC-active periods and (b) TC-inactive periods of 1979–2021, and (c) the associated differences between TC-active periods and TC-inactive periods of 1979–2021. The red rectangle indicates the target area presented in Fig. 1b.

where m is the mass of the air parcel a; e_a and p_a are evaporation and precipitation rates, respectively; Δt (6 h in this study) is the time step of the backward tracking; and Δq_t is the specific humidity changes from time $t - \Delta t$ to t.

Before arriving at the target region, an air parcel may undergo multiple uptakes and releases of moisture, making the moisture contributions of source regions far away from the target area much less than those of regions around the
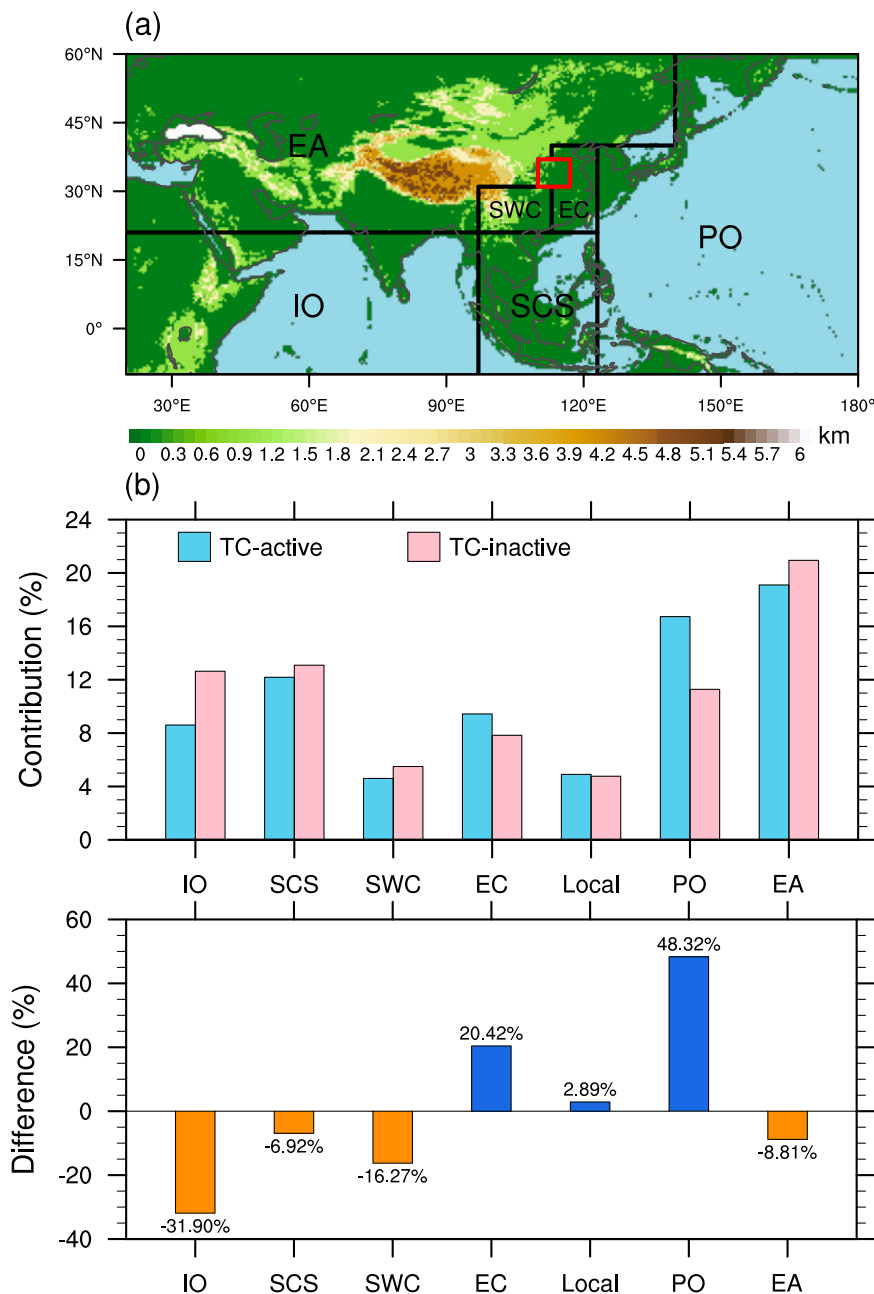
FIG. 5. (a) Distribution of the seven relevant moisture sources used in the present study. Shadings indicate the topography. IO, SCS, PO, SWC, EC, Local, and EA represent the Indian Ocean, the South China Sea, the Pacific Ocean, Southwest China, East China, the local area, and Eurasia, respectively. (b) Moisture contributions from the seven sources to the total moisture of rainfall over Henan Province during the TC-active periods (sky-blue columns) and TC-inactive periods (pink columns) and the associated differences (dark-orange and royal-blue columns) between the two periods.

target area (Sodemann et al. 2008). Therefore, to quantify moisture contributions from different sources to the precipitation in the study area, we apply a source attribution method proposed by Sodemann et al. (2008). The details are as follows:

1) The effective change in specific humidity, denoted as Q_t, is set to zero when the evaporation rate is less than or equal to the precipitation rate ($e_t - p_t \leq 0$).

2) Q_t is temporarily set to Δq_t when $e_t - p_t > 0$. The calculation of the final Q_t depends on moisture budget of all

time after time t, excluding the final time reached the target grid. For any time t' after time t, if $\Delta q_{t'} < 0$, Q_t is proportionally decreased as follows:

$$Q_t = \Delta q_t \times \frac{q'_t}{q_{t'-\Delta t}}. \tag{3}$$

When $\Delta q_{t'} > 0$ maintained, Q_t is kept equal to Δq_t.

3) The effective water vapor contribution ratio from region A to the target area CR(A) can be express as the following formula:

$$\text{CR}(A) = \frac{\sum Q(A)}{\sum Q_{t=-6}} \times 100\%, \tag{4}$$

where $\sum Q_{t=-6}$ is the total moisture content of all air parcels at the time of last 6 h before arriving at the target area, and $\sum Q(A)$ is the total of effective changes in specific humidity at region A.

3. The influence of TC on moisture contributions for rainfall over Henan Province

The averaged geopotential height at 500 hPa and the moisture flux at 850 hPa over East Asia for all TC-active and TC-inactive periods during July–August of 1979–2021 are shown in Fig. 2. Compared with TC-inactive periods, the intensity of WNPSH is significantly weakened during TC-active periods, with the western edge of WNPSH (represented by the contour line of 588 dagpm) moving eastward to nearly 136°E. Meanwhile, a pair of anomaly cyclone, centered to the east of Taiwan island, and anticyclone, centered over the Japan Sea, can be observed south and north of about 32°N (Fig. 2c). As a result, an abnormal easterly airflow is seen in the lower troposphere (850 hPa) from the WNP to East China during TC-active periods. Meanwhile, there is a significant anomaly moisture flux from the Pacific Ocean, with its maximum reaching 0.06 m s^{-1} kg kg^{-1} (Fig. 2c).

We further investigate the moisture transport for the July–August precipitation over Henan Province using the HYSPLIT model. There are roughly three moisture pathways (Figs. 3a,b)—the southwesterly path from the Bay of Bengal (BoB; path 1), the southeasterly path from the WNP (path 2), and the westerly path from the Mediterranean (path 3)—in the mean states of both periods (TC-active and TC-inactive periods). Path 1 brings moisture from the Indian Ocean to Henan via the Indo-China Peninsula and South China. Moisture from the Pacific Ocean (path 2) is transported to Henan Province via eastern China. Moisture from the Mediterranean (path 3) experiences a relatively long journey to the target area. These air parcels travel through west and central Asia, Siberia, and Mongolia before they reach Henan. The trajectory frequency differences between TC-active and TC-inactive periods are shown in Fig. 3c. The trajectory frequency from the Pacific Ocean is notably higher during the TC-active periods than that during the TC-inactive periods due to circulation differences, which are consistent with the anomalous easterly wind in Fig. 2c. In contrast, the trajectory frequency from the BoB is significantly reduced in
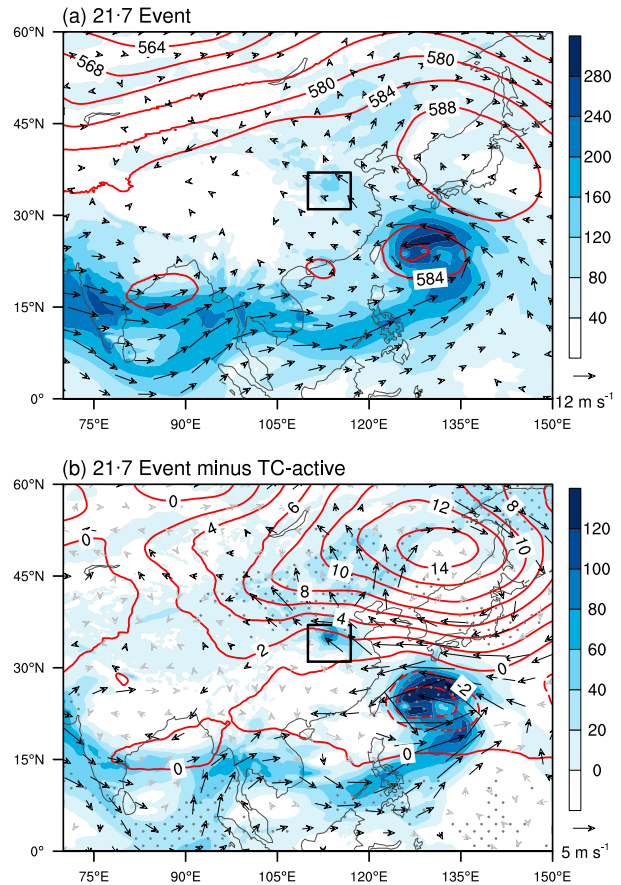

FIG. 6. Spatial distributions of mean geopotential height (contours; unit: dagpm) at 500 hPa, moisture flux (shading; unit: 10^{-3} m s^{-1} kg kg^{-1}), and horizontal wind fields (vectors; unit: m s^{-1}) at 850 hPa over East Asia during (a) the "21·7" event and (b) the associated differences between the "21·7" event and the TC-active periods. Dotted regions in (b) present the 99% confidence level for geopotential height at 500 hPa and moisture flux at 850 hPa, and black vectors in (b) present the 99% confidence level for horizontal wind fields at 850 hPa based on Student's t test. The black solid rectangle indicates the location of Henan Province which is presented in Fig. 1b.

TC-active periods. The trajectories from the Mediterranean are comparable for both periods, which is consistent with the less evident circulation differences over the mid–high latitudes of East Asia (Fig. 2c).

To quantify the moisture contributions of relevant sources to the precipitation in the target area and the differences between the two periods, we use the source attribution method (Sodemann et al. 2008). Figures 4a and 4b show the distributions of fractional moisture contribution for each 1° × 1° grid box during the TC-active and TC-inactive periods, respectively. It is not surprising to see that the grid boxes closer to the target area tend to have larger moisture contributions since they experienced less loss and obtain cycles of moisture due to the short distance. In our case, the region with higher moisture contributions stretches southward from the Henan Province, which is tightly linked with the mean southwesterly
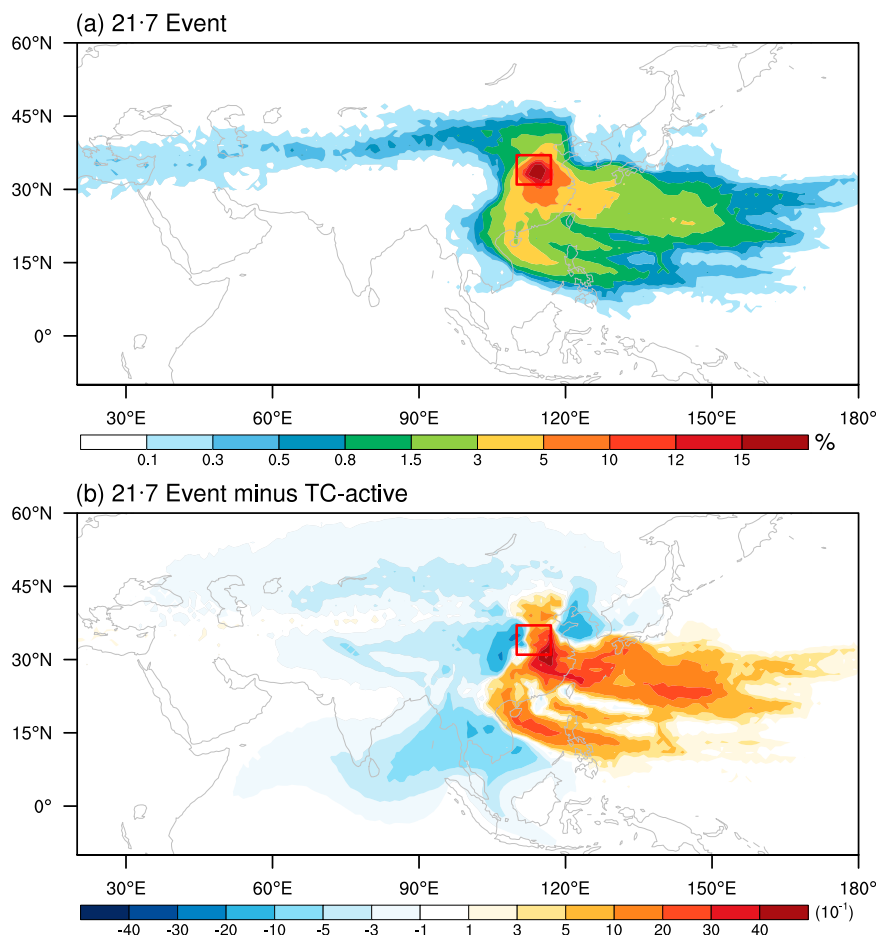
FIG. 7. Spatial distribution of the effective trajectory frequency (shading; unit: %) during (a) the "21·7" event and (b) the associated differences between the "21·7" event and TC-active periods of 1979–2021. The red rectangle indicates the area presented in Fig. 1b.

monsoon circulation. Comparing the TC-active and TC-inactive periods, there is an obvious dipole pattern of anomaly moisture contribution with southwestward contributions reduced and southeastward contributions enhanced during TC-active periods (Fig. 4c). The anomaly dipole pattern coincides with the anomaly cyclonic circulation in TC-active periods (cf. Figs. 4c and 2c).

To quantify the influence of TC on moisture contributions from different source regions, moisture contributions for seven subregions (Fig. 5a) are calculated, including the Indian Ocean (IO), the South China Sea and its adjacent area (SCS), the Pacific Ocean (PO), Southwest China (SWC), East China (EC), Eurasia (EA), and local area (Local). The moisture contributions and the associated differences between the TC-active periods and the TC-inactive periods are shown in Fig. 5b. Compared with the TC-inactive periods, moisture contributions from the PO, EC, and Local regions increase, while those from the other four moisture sources decrease. The maximum increase in amplitude by 48.32% (16.73% versus 11.28%) is observed over the PO. For EC, its moisture contribution increases from 7.84% to 9.44%, with a magnitude of 20.42% during the

TC-active periods. The fractional increase in moisture contributions from Local is relatively low (2.89%). On the other hand, the total moisture contribution from the IO and the SWC, along the southwesterly moisture path of Henan Province, is reduced from 18.13% to 13.21%, with the maximum decrease magnitude of −31.90% (12.64% versus 8.61%) over the IO. Meanwhile, the EA also shows a considerable moisture decrease by −8.81%, while the fractional change in moisture contributions from SCS is relatively low (−6.92%).

4. How extreme is the "21·7" event in moisture transport?

During the "21·7" event, the TC Infa helped establish the easterly moisture channel and contributed to the intensification of the extreme precipitation (Fig. 6a; Yin et al. 2022; X. Zhang et al. 2021). Relative to the mean state of the TC-active periods, the anomaly easterly moisture flux, between the TC Infa and the northward WNPSH, could reach 0.1 m s^{-1} kg kg^{-1} or more. Indeed, the observed low-level easterly jet, rather than the southwesterly flow in the mean state, becomes the main
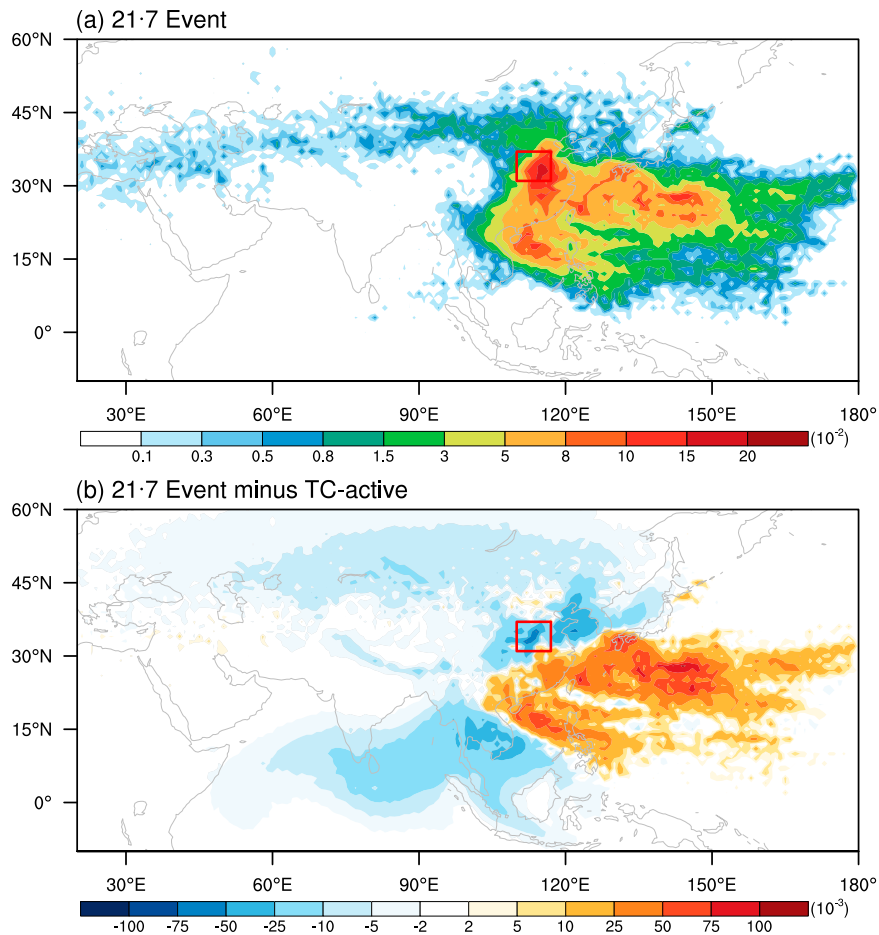
FIG. 8. The moisture contribution (shading; units: %) to Henan Province during (a) the "21·7" event and (b) the associated differences between the "21·7" event and TC-active periods of 1979–2021. The red rectangle indicates the area presented in Fig. 1b.

moisture channel (Fig. 6b), as also noted by previous studies (Ran et al. 2021; Yin et al. 2022; S. Zhang et al. 2021). The quantitative details of moisture transport for this event are shown in Fig. 7. Compared with the TC-active periods, substantial increases in moisture trajectories are observed for the easterly and southeasterly channels during the "21·7" event (Fig. 8). Overall, the trajectory frequency over PO and EC is sharply increased, while the frequency over IO is significantly decreased.

The fractional moisture contribution of PO is enormously increased to 37.87% (Fig. 9), ranking first in the seven source regions, with an increase amplitude of 126.32% compared with the mean state during TC-active periods. In contrast, moisture contribution from the IO is sharply reduced by 98.26%, to a nearly negligible level (0.15%) during this event (Fig. 9). Moreover, moisture contributions of the EA, Local, and SCS all decrease significantly by 71.15% (5.51% versus 19.10%), 19.94% (3.93% versus 4.91%), and 16.51% (10.17% versus 12.18%), respectively. The fractional moisture contributions of EC and SWC during the "21·7" event are comparable to the mean state of the TC-active periods, with changes of about 5%.

We apply a bootstrap (Efron and Tibshirani 1994) technique to provide a statistical analysis on how TCs modulate moisture transport supplied for precipitation in Henan Province on a time scale of several days. This also helps us establish how extreme the moisture transport during the "21·7" event was. Since the "21·7" event lasted for 6 days, all the effective trajectories obtained during the TC-active period in July–August from 1979 to 2021 are resampled into equivalent 6-day blocks. Overall, we generate 10 000 6-day samples, with each 6-day block consisting of 24 randomly selected 6-h outputs with replacement, including their three-dimensional locations and specific humidity. A similar procedure is applied for the TC-inactive periods. To highlight the regions with the most significant moisture contribution increase (PO) and decrease (IO), we calculate moisture contributions from the PO and IO during TC-active and TC-inactive periods for all 10 000 samples, and their resulting probability distribution functions (PDFs; Fig. 10). The PDFs all look like normal distributions, suggesting 10 000 times resampling is large enough to provide statistically significant analysis.
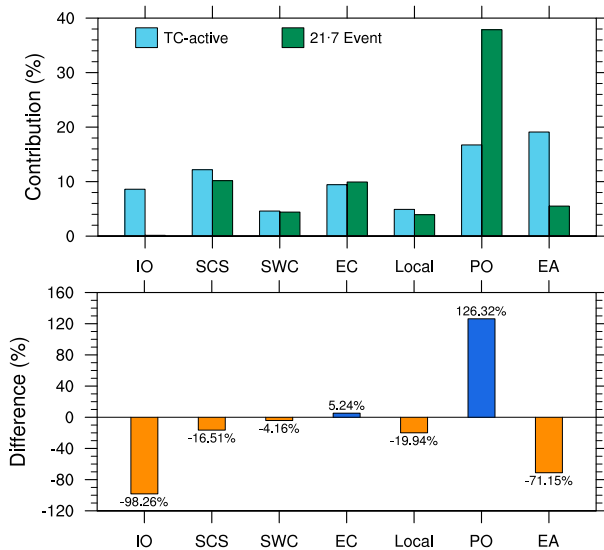
FIG. 9. Moisture contributions from the seven sources (divided as in Fig. 5a) to the total moisture of the rainfall over Henan Province during the "21·7" event (sea-green columns) and TC-active periods (sky-blue columns) and the associated differences (dark-orange and royal-blue columns) between the "21·7" event and TC-active periods.
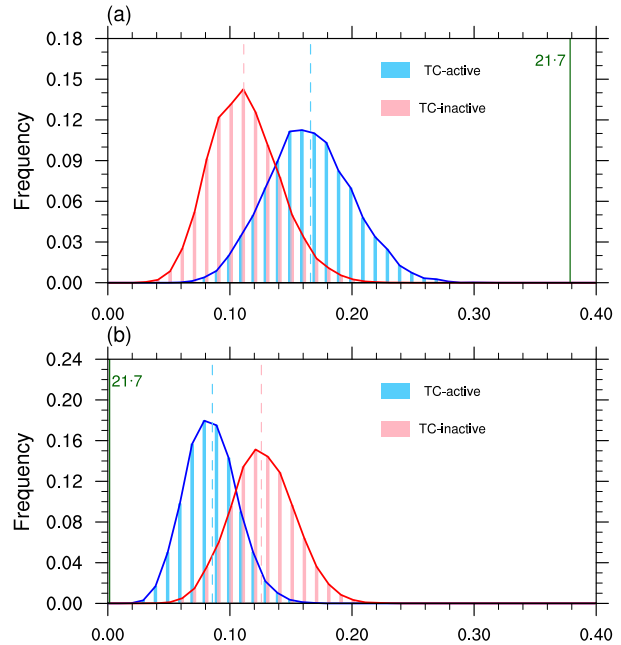

FIG. 10. Histograms of moisture contributions from the (a) PO and (b) IO based on the 10 000 samples of the same 6-day blocks, consisting of 24 times of 6-h results, the same as the time scale of the "21·7" event, using the bootstrap resampling (with replacement) technique during TC-active (sky-blue bars) and TC-inactive (pink bars) periods. The sky-blue and pink dashed lines demonstrate the mean value, and dark-green lines indicate the corresponding moisture contribution during the "21·7" event.

For moisture contributions from the PO, the mean values of the distributions are 16.60% and 11.13% (Fig. 10a), respectively, for the TC-active and TC-inactive periods. These are comparable to the composite mean values, i.e., 16.73% and 11.28% (Fig. 5b), for the whole period as illustrated above. The corresponding standard deviations (σ) are 3.48% and 2.82%, respectively. Compared to the TC-inactive periods, the moisture contributions PDF from the PO for the TC-active periods shows a shift of the mean value to the higher side with an insignificant difference in variance. For the "21·7" event, the PO accounted for 37.87% of moisture contribution (Fig. 9), which falls outside the $+6\sigma$ for the range of TC-active and (of course) TC-inactive PDFs, so the occurrence probability for such an event is less than 10^{-6}.

A similar procedure is applied to evaluate moisture contributions from the IO. In contrast with the PO, the PDFs in moisture contributions of the IO show a significant shift of the mean value to the lower side (8.56% versus 12.58%) during the TC-active relative to TC-inactive periods (Fig. 10b). The corresponding standard deviations (σ) are 2.13% and 2.60% during the TC-active and TC-inactive periods, respectively. During the "21·7" event, the moisture contribution from the IO (0.15%) falls far outside the -3σ from the mean of the distributions for the TC-active and -4σ from the TC-inactive PDFs. Therefore, we may safely conclude that for a 6-day time scale, TC activities could significantly modulate moisture transport supplied for precipitation over Henan, with a significant increase of contributions from the PO. We conclude that, in terms of the moisture contribution from the PO, the "21·7" event is a rare and extreme event, with the occurrence probability being less than one in a million times.

5. Conclusions and discussion

Changes in sources and paths of moisture for precipitation over North China's Henan Province associated with the activities of tropical cyclones (TCs) are not well understood. Using the HYSPLIT model, we quantified TC-related changes in moisture sources and paths for precipitation over Henan by a comparison between the TC-active and TC-inactive periods during July–August, 1979–2021. Moreover, the moisture transport of the "21·7" catastrophic extreme rainfall event over Henan is also analyzed. The major conclusions are as follows.

Compared to the TC-inactive periods, the western North Pacific subtropical high (WNPSH) is weakened during TC-active periods (Zhong et al. 2019), with the western ridge shifting eastward to about 136°E on average. Correspondingly, anomaly easterly winds are observed over eastern China and the adjacent oceans in the lower troposphere. As a result, the moisture transport flux from the Pacific Ocean (PO) is enhanced during TC-active periods.

Using the HYSPLIT model, we show that there are roughly three moisture paths for precipitation over the Henan Province from the Bay of Bengal (BoB), WNP, and the Mediterranean. Accordingly, compared with TC-inactive periods, the anomaly pattern in moisture contribution during TC-active periods is demonstrated as a west–east dipole. Moisture contributions from the PO, eastern China and the adjacent oceans (EC), and the local area (Local) increased by 48.32%,

20.42%, and 2.89%, respectively, while those from the Indian Ocean (IO), Southwest China (SWC), Eurasia (EA), and South China Sea (SCS) are decreased by 31.9%, 16.27%, 8.81%, and 6.92%, respectively.

Furthermore, we investigate the role of TC Infa in modulating moisture transport in the catastrophic "21·7" extreme rainfall event. Compared to the mean of the TC-active periods, moisture contribution from PO is substantially enhanced with an amplitude of 126.32%, while those from the IO and EA are substantially reduced, with a maximum amplitude of -98.26% observed over the IO. Using a bootstrap method (with replacement), we generated 10 000 samples of the same 6-day blocks as the "21·7" event. Using this synthetic dataset, we show that moisture contributions from the PO and IO for the "21·7" event fall outside the $+6\sigma$ and -3σ range, respectively, for the TC-active and TC-inactive probability distributions. We further define the PSTC-active period as the time when a TC is observed over the Philippine Sea (19°–27°N, 124°–135°E), consistent with the area Typhoon Infa remained in during the "21·7" event. A similar bootstrap procedure in section 4 is applied for the PSTC-active period to examine the influence of the TCs, with locations similar to the Typhoon Infa, on the moisture transport for the "21·7" event (Fig. S2). Moisture contributions from the PO and IO for the "21·7" event fall outside the $+6\sigma$ and -4σ range, respectively, for the PSTC-active probability distributions, which is similar to the results for the TC-active and TC-inactive probability distributions. Thus, in terms of moisture contribution from the PO, the "21·7" event is a rarely seen extreme event in moisture transport.

Moreover, we have also calculated the moisture contribution only when air parcels are below the boundary layer. Overall, the moisture contributions below the boundary layer account for about 10%–40% of all moisture calculated from the whole atmosphere. Note that the main results remain unchanged with those derived from the whole atmosphere (Figs. S3–S7). Also, due to the effect of complex terrain, uncertainties exist in moisture transport calculation, especially for long-distance moisture transport across mountainous regions such as Southwest China.

In this study, we mainly focus on the differences in moisture contributions between TC-active and TC-inactive periods to precipitation in Henan, but we should note that the "21·7" extreme event is under extremely favorable conditions, with not only the TC activities, but also the northward movement of WNPSH and the special terrain topography of Henan Province. Though we have shown that substantial changes in moisture transport could be associated with TC activities, such large-scale condition change does not guarantee the occurrence of extreme rainfall events. Furthermore, in terms of changes in moisture transport associated with typhoon activities, further works need to be done such as to what extent and how the changed moisture pathways and contributions would influence the total moisture convergence, the mesoscale development, and hence the extreme precipitation.

REFERENCES

Arakane, S., H.-H. Hsu, C.-Y. Tu, H.-C. Liang, Z.-Y. Yan, and S.-J. Lin, 2019: Remote effect of a tropical cyclone in the Bay of Bengal on a heavy-rainfall event in subtropical East Asia. *npj Climate Atmos. Sci.*, **2**, 25, https://doi.org/10.1038/s41612-019-0082-8.

Bao, X., and Coauthors, 2015: Diagnostics for an extreme rain event near Shanghai during the landfall of Typhoon Fitow (2013). *Mon. Wea. Rev.*, **143**, 3377–3405, https://doi.org/10.1175/MWR-D-14-00241.1.

Chang, C.-P., Y.-T. Yang, and H.-C. Kuo, 2013: Large increasing trend of tropical cyclone rainfall in Taiwan and the roles of terrain. *J. Climate*, **26**, 4138–4147, https://doi.org/10.1175/JCLI-D-12-00463.1.

Chen, L. S., Z. Y. Meng, and C. H. Cong, 2017: An overview on the research of typhoon rainfall distribution (in Chinese). *J. Mar. Meteor.*, **37**, 1–7.

Chen, Y., and Y. Luo, 2018: Analysis of paths and sources of moisture for the South China rainfall during the presummer rainy season of 1979–2014. *J. Meteor. Res.*, **32**, 744–757, https://doi.org/10.1007/s13351-018-8069-7.

Deng, D., N. E. Davidson, L. Hu, K. J. Tory, M. C. N. Hankinson, and S. Gao, 2017: Potential vorticity perspective of vortex structure changes of Tropical Cyclone Bilis (2006) during a heavy rain event following landfall. *Mon. Wea. Rev.*, **145**, 1875–1895, https://doi.org/10.1175/MWR-D-16-0276.1.

Ding, Y., 2015: On the study of the unprecedented heavy rainfall in Henan Province during 4–8 August 1975: Review and assessment (in Chinese). *Acta Meteor. Sin.*, **73**, 411–424, https://doi.org/10.11676/qxxb2015.067.

——, and J. C. L. Chan, 2005: The East Asian summer monsoon: An overview. *Meteor. Atmos. Phys.*, **89**, 117–142, https://doi.org/10.1007/s00703-005-0125-z.

Draxler, R. R., and G. D. Hess, 1998: An overview of the HYSPLIT_4 modelling system for trajectories. *Aust. Meteor. Mag.*, **47**, 295–308.

Eagleson, P. S., 1970: *Dynamic Hydrology.* McGraw-Hill, 462 pp.

Efron, B., and R. J. Tibshirani, 1994: *An Introduction to the Bootstrap.* Chapman and Hall, 456 pp.

Franco-Díaz, A., N. P. Klingaman, P. L. Vidale, L. Guo, and M.-E. Demory, 2019: The contribution of tropical cyclones to the atmospheric branch of Middle America's hydrological cycle using observed and reanalysis tracks. *Climate Dyn.*, **53**, 6145–6158, https://doi.org/10.1007/s00382-019-04920-z.

Guo, L., N. P. Klingaman, P. L. Vidale, A. G. Turner, M.-E. Demory, and A. Cobb, 2017: Contribution of tropical cyclones to atmospheric moisture transport and rainfall over East Asia. *J. Climate*, **30**, 3853–3865, https://doi.org/10.1175/JCLI-D-16-0308.1.

Gustafsson, M., D. Rayner, and D. Chen, 2010: Extreme rainfall events in southern Sweden: Where does the moisture come from? *Tellus*, **62A**, 605–616, https://doi.org/10.1111/j.1600-0870.2010.00456.x.

Hersbach, H., and Coauthors, 2020: The ERA5 global reanalysis. *Quart. J. Roy. Meteor. Soc.*, **146**, 1999–2049, https://doi.org/10.1002/qj.3803.

Huang, Y., and X. Cui, 2015a: Moisture sources of an extreme precipitation event in Sichuan, China, based on the Lagrangian method. *Atmos. Sci. Lett.*, **16**, 177–183, https://doi.org/10.1002/asl2.562.

——, and ——, 2015b: Moisture sources of torrential rainfall events in the Sichuan basin of China during summers of 2009–13. *J. Hydrometeor.*, **16**, 1906–1917, https://doi.org/10.1175/JHM-D-14-0220.1.

Izquierdo, R., A. Avila, and M. Alarcón, 2012: Trajectory statistical analysis of atmospheric transport patterns and trends in precipitation chemistry of a rural site in NE Spain in 1984–2009. *Atmos. Environ.*, **61**, 400–408, https://doi.org/10.1016/j.atmosenv.2012.07.060.

Jiang, H., and E. Zipser, 2010: Contribution of tropical cyclones to the global precipitation from eight seasons of TRMM data: Regional, seasonal, and interannual variations. *J. Climate*, **23**, 1526–1543, https://doi.org/10.1175/2009JCLI3303.1.

Lin, X., Z. Wen, W. Zhou, R. Wu, and R. Chen, 2017: Effects of tropical cyclone activity on the boundary moisture budget over the eastern China monsoon region. *Adv. Atmos. Sci.*, **34**, 700–712, https://doi.org/10.1007/s00376-017-6191-6.

Liu, L., and Y. Wang, 2020: Trends in landfalling tropical cyclone–induced precipitation over China. *J. Climate*, **33**, 2223–2235, https://doi.org/10.1175/JCLI-D-19-0693.1.

Luo, Y., M. Wu, F. Ren, J. Li, and W.-K. Wong, 2016: Synoptic situations of extreme hourly precipitation over China. *J. Climate*, **29**, 8703–8719, https://doi.org/10.1175/JCLI-D-16-0057.1.

——, J. Zhang, M. Yu, X. Liang, R. Xia, Y. Gao, X. Gao, and J. Yin, 2023: On the influences of urbanization on the extreme rainfall over Zhengzhou on 20 July 2021: A convection-permitting ensemble modeling study. *Adv. Atmos. Sci.*, **40**, 393–409, https://doi.org/10.1007/s00376-022-2048-8.

Martius, O., and Coauthors, 2013: The role of upper-level dynamics and surface processes for Pakistan flood of July 2010. *Quart. J. Roy. Meteor. Soc.*, **139**, 1780–1797, https://doi.org/10.1002/qj.2082.

Nieto, R., D. Ciric, M. Vazquez, M. L. R. Liberato, and L. Gimeno, 2019: Contribution of the main moisture sources to precipitation during extreme peak precipitation months. *Adv. Water Resour.*, **131**, 103385, https://doi.org/10.1016/j.advwatres.2019.103385.

Prat, O. P., and B. R. Nelson, 2013: Mapping the world's tropical cyclone rainfall contribution over land using the TRMM multi-satellite precipitation analysis. *Water Resour. Res.*, **49**, 7236–7254, https://doi.org/10.1002/wrcr.20527.

——, and ——, 2016: On the link between tropical cyclones and daily rainfall extremes derived from global satellite observations. *J. Climate*, **29**, 6127–6135, https://doi.org/10.1175/JCLI-D-16-0289.1.

Ran, L., and Coauthors, 2021: Observational analysis of the dynamic, thermal, and water vapor characteristics of the "7.20" extreme rainstorm event in Henan Province, 2021 (in

Chinese). *Chin. J. Atmos. Sci.*, **45**, 1366–1383, https://doi.org/10.3878/j.issn1006-9895.2109.21160.

Ren, F., G. Wu, W. Dong, X. Wang, Y. Wang, W. Ai, and W. Li, 2006: Changes in tropical cyclone precipitation over China. *Geophys. Res. Lett.*, **33**, L20702, https://doi.org/10.1029/2006GL027951.

Rodgers, E. B., R. F. Adler, and H. F. Pierce, 2001: Contribution of tropical cyclones to the North Atlantic climatological rainfall as observed from satellites. *J. Appl. Meteor. Climatol.*, **40**, 1785–1800, https://doi.org/10.1175/1520-0450(2001)040<1785:COTCTT>2.0.CO;2.

Salih, A. A. M., Q. Zhang, and M. Tjerström, 2015: Lagrangian tracing of Sahelian Sudan moisture sources. *J. Geophys. Res. Atmos.*, **120**, 6793–6808, https://doi.org/10.1002/2015JD023238.

Schumacher, R. S., T. J. Galarneau, and L. F. Bosart, 2011: Distant effects of a recurving tropical cyclone on rainfall in a midlatitude convective system: A high-impact predecessor rain event. *Mon. Wea. Rev.*, **139**, 650–667, https://doi.org/10.1175/2010MWR3453.1.

Shi, Y., Z. Jiang, Z. Liu, and L. Li, 2020: A Lagrangian analysis of water vapor sources and pathways for precipitation in East China in different stages of the East Asian summer monsoon. *J. Climate*, **33**, 977–992, https://doi.org/10.1175/JCLI-D-19-0089.1.

Sodemann, H., and A. Stohl, 2013: Moisture origin and meridional transport in atmospheric rivers and their association with multiple cyclones. *Mon. Wea. Rev.*, **141**, 2850–2868, https://doi.org/10.1175/MWR-D-12-00256.1.

——, C. Schwierz, and H. Wernli, 2008: Interannual variability of Greenland winter precipitation sources: Lagrangian moisture diagnostic and North Atlantic Oscillation influence. *J. Geophys. Res.*, **113**, D03107, https://doi.org/10.1029/2007JD008503.

Stein, A. F., R. R. Draxler, G. D. Rolph, B. J. B. Stunder, M. D. Cohen, and F. Ngan, 2015: NOAA's HYSPLIT atmospheric transport and dispersion modeling system. *Bull. Amer. Meteor. Soc.*, **96**, 2059–2077, https://doi.org/10.1175/BAMS-D-14-00110.1.

Stohl, A., and P. James, 2004: A Lagrangian analysis of the atmospheric branch of the global water cycle. Part I: Method description, validation, and demonstration for the August 2002 flooding in central Europe. *J. Hydrometeor.*, **5**, 656–678, https://doi.org/10.1175/1525-7541(2004)005<0656:ALAOTA>2.0.CO;2.

——, and ——, 2005: A Lagrangian analysis of the atmospheric branch of the global water cycle. Part II: Moisture transports between Earth's ocean basins and river catchments. *J. Hydrometeor.*, **6**, 961–984, https://doi.org/10.1175/JHM470.1.

Sun, B., and H. Wang, 2014: Moisture sources of semiarid grassland in China using the Lagrangian particle model FLEXPART. *J. Climate*, **27**, 2457–2474, https://doi.org/10.1175/JCLI-D-13-00517.1.

Villarini, G., and R. F. Denniston, 2016: Contribution of tropical cyclones to extreme rainfall in Australia. *Int. J. Climatol.*, **36**, 1019–1025, https://doi.org/10.1002/joc.4393.

Wang, C.-C., H.-C. Kuo, R. H. Johnson, C.-Y. Lee, S.-Y. Huang, and Y.-H. Chen, 2015: A numerical study of convection in rainbands of Typhoon Morakot (2009) with extreme rainfall: Roles of pressure perturbations with low-level wind maxima. *Atmos. Chem. Phys.*, **15**, 11 097–11 115, https://doi.org/10.5194/acp-15-11097-2015.

Wen, Y., L. Xue, Y. Li, N. Wei, and A. M. Lü, 2015: Interaction between Typhoon Vicente (1208) and the western Pacific subtropical high during the Beijing extreme rainfall of 21 July 2012. *J. Meteor. Res.*, **29**, 293–304, https://doi.org/10.1007/s13351-015-4097-8.

Yang, L., M. Liu, J. A. Smith, and F. Tian, 2017: Typhoon Nina and the August 1975 flood over central China. *J. Hydrometeor.*, **18**, 451–472, https://doi.org/10.1175/JHM-D-16-0152.1.

Yin, J., H. Gu, X. Liang, M. Yu, J. Sun, Y. Xie, F. Li, and C. Wu, 2022: A possible dynamic mechanism for rapid production of the extreme hourly rainfall in Zhengzhou City on 20 July 2021. *J. Meteor. Res.*, **36**, 6–25, https://doi.org/10.1007/s13351-022-1166-7.

Yoshida, K., and H. Itoh, 2012: Indirect effects of tropical cyclones on heavy rainfall events in Kyushu, Japan, during the baiu season. *J. Meteor. Soc. Japan*, **90**, 377–401, https://doi.org/10.2151/jmsj.2012-303.

Zhang, D.-L., Y. Lin, P. Zhao, X. Yu, S. Wang, H. Kang, and Y. Ding, 2013: The Beijing extreme rainfall of 21 July 2012: "Right results" but for wrong reasons. *Geophys. Res. Lett.*, **40**, 1426–1431, https://doi.org/10.1002/grl.50304.

Zhang, S., B. Liu, G. Ren, T. Zhou, C. Jiang, S. Li, and B. Su, 2021: Moisture sources and paths associated with warm-season precipitation over the Sichuan basin in southwestern China: Climatology and interannual variability. *J. Hydrol.*, **603**, 127019, https://doi.org/10.1016/j.jhydrol.2021.127019.

Zhang, X., H. Yang, X. Wang, L. Shen, D. Wang, and H. Li, 2021: Analysis on characteristic and abnormality of atmospheric circulations of the July 2021 extreme precipitation in Henan. *Trans. Atmos. Sci.*, **44**, 672–687, https://doi.org/10.13878/j.cnki.dqkxxb.20210907001.

Zhong, Z., X. Chen, X.-Q. Yang, Y. Ha, and Y. Sun, 2019: The relationship of frequent tropical cyclone activities over the western North Pacific and hot summer days in central-eastern China. *Theor. Appl. Climatol.*, **138**, 1395–1404, https://doi.org/10.1007/s00704-019-02908-7.